International Journal of Mechanical Engineering and Technology (IJMET)
Volume 10, Issue 1, January 2019, pp. 119–132, Article ID: IJMET_10_01_012
Available online at http://www.iaeme.com/ijmet/issues.asp?JType=IJMET&VType=10&IType=1
ISSN Print: 0976-6340 and ISSN Online: 0976-6359

NUMERICAL SIMULATION OF LAMINAR INCOMPRESSIBLE DRIVEN CAVITY FLOW IN A L-SHAPE DOMAIN

Dr. Abbas Alwi SakhirAbed
University of AL-Qadisiyah -College of Engineering, Iraq

ABSTRACT

Two-dimensional laminar incompressible flow governing equation is solved numerically to gain insight into flow separation and recirculation of flow processes in an L-shape lid driven cavity. Stream function vorticity formulation of Navier-Stokes equation is solved with clustered grids on physical domain. The hydrodynamic study is carried out for different Reynolds number. It is found that at Re ≥ 600 primary vortex center becomes independent of Reynolds number. Velocity contours are presented for different

Reynolds number. The wall vorticity is sensitive in the upstream of the moving lid. The skin friction coefficient is less affected at deeper cavity location.

Keywords: L-Shape Lid Driven Cavity, Vortex Flow, Wall Vorticity, Velocity Vector.

Cite this Article: Dr. Abbas Alwi SakhirAbed, Numerical Simulation of Laminar Incompressible Driven Cavity Flow In A L-Shape Domain, International Journal of Mechanical Engineering and Technology, 9(13), 2018, pp. 119–132.
http://www.iaeme.com/ijmet/issues.asp?JType=IJMET&VType=9&IType=13

Nomenclature

i: x-direction grid point
j: y-direction grid point
n: Normal direction
Re Reynolds number for the fluid, dimensionless
$\bar{t}$: Dimensional time, s
t: nondimensional time
$\bar{u},\bar{v}$: Dimensional velocity components along (x; y) axes, m/s
u; v: Dimensionless velocity components along (x; y) axes
U: moving plate velocity, m/s

W: width of the lid, m

$\bar{x}, \bar{y}$: Dimensional Cartesian co-ordinates, m

x; y: dimensionless Cartesian co-ordinates

Greek symbols

E: convergence criterion

K: clustering parameter

ψ: dimensionless stream function

ω: dimensionless vorticity

Subscripts

max: maximum

W: wall

1. INTRODUCTION

L-shape problems are very common in many industrial situations like heat exchanger, cooling turbine, sheet metal coating, electronics cooling and many others. For the present investigation L-shape lid driven cavity is studied in detail. L-shape domain is having variety of applications [1]. Lid driven cavity problem is extensively studied because of its certain flow features. Boundary layer on the wall, flow separation from one wall and reattachment on the perpendicular wall, attachment and separation from the same wall, multiple separation and attachment, vortices, bubbles are some interesting features of this problem. Almost all numerical methods for fluid flow developed are tested with this problem for accuracy. Probably the rest systematic numerical study of square lid driven cavity flow problem was given by Burggraf [2]. Using a stream function vorticity formulation, he was able to predict upto Reynolds number (Re) = 400 and compared the result with Batchelor's model. Nallasamy and Prasad [3] investigated the problem for Re = 0-50000. They have used unsteady stream function vorticity formulation and ADI (Alternating Direction Implicit) with higher order up winding scheme. However their results are limited by the choice of less number of grids which gave an under resolved solution. In spite of that, they were able to predict qualitatively the appearance and relative size of the primary and secondary vortices. Ghia et al.'s [4] work is usually considered a benchmark solution for validating numerical schemes. In their work, multigrid stream function formulation is used in the transient form of equation. Cortes and Miller [5] studied the lid driven cavity problem for aspect ratio equal to 1 and 2 in primitive variable formulation. They have observed that in case of square cavity, the flow attains an unsteady state for Re = 10,000. However detailed results are not provided. Liao and Zhu [6] have solved in streamfunction and vorticity formulation steady state equations. They have reported steady state solution upto Re = 10000. Two sided lid driven cavity is studied by Oztop and Dagtekin [7]. For various lid moving direction mixed convection heat transfer results are presented. Recently Podvin et al [8] studied flow past an open cavity using reconstruction method. POD (proper orthogonal decomposition) based 2D and 3D simulations are carried out for open cavity. The above literature study shows the interest on lid driven problem is very keen by the researcher. They reported transient as well as steady state natural convection results for different Rayleigh number and length to width ratio. Also they tested for different thermal boundary conditions. They found that for certain boundary conditions the steady state does not exist. Laminar natural convection study is carried out for heated backward step on similar L-shape domain by Chang and Tsay [10]. The exact of Rayleigh number, Prandtl number and effect of geometry are reported in terms of isotherm,

streamfunction contour and local Nusselt number. Effect of Grash of number and inter wall spacing are reported by Mahmud [1] for L-shaped cavity. Oosterlee el al. [9] solved L-shape lid driven cavity problem to validate numerical procedure and presented centerline velocity value for Re = 100 and Re = 1000 only. Kulsri et al [10] verified their new method by simulating various shape of cavity viz. rectangular, half-circular and beer bucket shaped. The available literature shows that the interesting flow physics of L-shape cavity is limited which motivates the present investigation. The detailed hydrodynamic study is carried out for finding the strength of eddies, velocity and skin friction coeffcient for different Reynolds number and different aspect ratio.

2. MATHEMATICAL FORMULATION AND NUMERICAL PROCEDURE

Incompressible two-dimensional laminar flow is considered for the computation. The governing Navier-Stokes equations are solved by stream function-vorticity formulation. The transient non-dimensional governing equations in the conservative form are Roache [11],

Stream function equation

$$\nabla^2\psi = -\omega \tag{1}$$

unsteady vorticity equation,

$$\frac{\partial\omega}{\partial t} + \frac{\partial(u\omega)}{\partial x} + \frac{\partial(v\omega)}{\partial y} = \frac{1}{Re}\nabla^2\omega \tag{2}$$

The boundary conditions needed for the numerical simulation have been prescribed in Fig. 1.

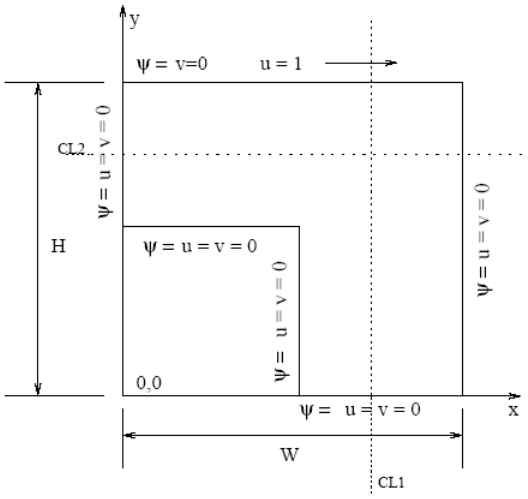

Figure I Schematic diagram and boundary conditions of L-Shape Lid driven cavity flow Program [9].

Streamfunction equation 1 is solved by Gauss Seidel method. The unsteady vorticity transport equation 2 in time is solved by Alternate Direction Implicit scheme (ADI). The central differencing scheme is followed for both the convective as well as the diffusive terms (Roache [11]). The details of the discretisation and numerical procedure can be found from Kanna and Das [12]. A point to note down is in ADI method while doing in either in *x* or *y* direction sweep number of points will vary along length and height. That is in *x* direction sweep upto *H*=2 unknowns are *imax*=2 to *imax*. From *H*=2 to *H* unknowns are 2 to *imax*. Similarly in *y* direction sweep upto *W*=2 unknowns are *jmax*=2 to *jmax*. From *W*=2 to *W*

unknowns are 2 to *jmax*. Solution approaches steady-state asymptotically while the time reaches infinity. The computational domain considered here is clustered cartesian grids. For unit length, the grid space at *ith* node is [13],

$$x_i = \left(\frac{i}{i_{max}} - \frac{\kappa}{\vartheta} sin\left(\frac{i\vartheta}{i_{max}} \right) \right) \quad (3)$$

where ϑ is the angle and κ is the clustering parameter. ϑ = 4¼ stretch grids at mid plane and both end of the domain. κ varies between 0 to 1. When it approaches 1, more points fall near the end. Here we used κ=0.7. For the computation, time step 0.001 is used for $Re \leq 100$ and 0.005 is used for higher *Re*. At steady state, the error reaches the asymptotic behavior. Here it is set as sum of vorticity error reduced to either the convergence criteria ε or large total time.

$$\sum_{i,j=1}^{i_{max} j_{max}} \left(\omega_{i,j}^{t+\triangle t} - \omega_{i,j}^{t} \right) < \varepsilon \quad (4)$$

Comini et al [14] and Kanna and Das [12] used low *Re* steady-state solution as initial guess value for high *Re* flow for stream function and vorticity. The same practice is followed here also.

3. VALIDATION OF THE CODE

To validate the developed code, the two-dimensional lid-driven square-cavity flow problem (Ghia et al. [4]) is solved and results are compared. It is found good agreement among the benchmark results [4] and the present solutions. Further left wall vorticity is compared with Barragy and Carey [15] (Figure 2). Results compared upto *Re* = 10000 and found good agreement upto this Reynolds number. Due to scarcity of experimental results of the present geometry the results are compared with Oosterlee *et al* [9]. Results are compared at two locations named CL1 and CL2 (Fig. 1). *u*- Velocity and *v*- velocity components at these locations are compared with [9] for *Re* = 100 and *Re* = 1000 (Fig. 3(a) - 3(d)) and excellent agreement is obtained and this validation is presented in Kanna and Das [16].

4. RESULTS AND DISCUSSION

Two dimensional laminar incompressible flows on L-shape lid driven cavity problem is solved for Reynolds number ranging from 1 to 1300. Grid independence test is carried out by arranging the maximum number of grids in both directions are 41 *x* 41, 61 *x* 61, 81 *x* 81, 101 *x* 101 and 121 *x* 121 for *Re* = 400. Based on minimum streamfunction value at the primary vortex center (Table I), grids 101 *x* 101 have been used for the entire computation. Typical grids are shown in Figure 4. From this the minimum grid space is generated is 0.00501. The results are presented in terms of streamline contour, velocity contour, velocity vector, and vorticity along moving plate. To obtain the transient results time independent test is carried out. Figure 5 shows the center line *v* velocity along CL2. Three different time step values are, 0.005, 0.001, and 0.0001 used to reach time *t* = 0.1. Variation is observed when time step value is decreased from 0.005 to 0.001. Further time step value is decreased to 0.0001 and it is noticed that there is no variation in the profile. It is concluded that the time step 0.0001 is used to find the transient results. Transient results are presented from Figure 6- Figure 8. The stream line contour is shown at different time level. When *t* approaches at *t* = 0.1 the primary vortex forms and located near to the center of the moving plate (Figure 6(a)). When time increase to *t* = 1 the primary vortex moves in the moving plate direction (Figure 6(b)). It is

noticed that the secondary vortex is not formed at t = 1. Further time is increased to 3, it is observed that the secondary vortex is formed near bottom of the left wall as well as bottom of right side wall (Figure 6(c)) nearly same size. The primary vortex is moving towards the intersection of CL1 and CL2. When time reaches 5 the secondary vortex near the right wall becomes larger than the secondary vortex near the left wall and its center tends towards right side wall (Figure 6(d)). When time increases from 10, 20 and 100 (Figure 6(e)-7(a)) all the vortices are become stable and positioned. The u velocity along CL1 at different time level is shown in Figure 7(b). It is noticed that when t = 20 the solution reaches steady state. This is very clear with kinetic energy study. However it is ensured by allowing the computation for t > 20. Figure 8 shows the convergence history of kinetic energy. The kinetic energy expression [17] is given by.

$$E(n \times \delta t) = (\sum_{(i,j)=(1,1)}^{(nx,ny)} [(u_{i,j}^n)^2 + (v_{i,j}^n)^2])^{\frac{1}{2}} \quad - \quad (5)$$

Fig. 8(a) shows the early stage of kinetic energy for *Re* = 400. Kinetic energy gradually increases as time increases. It is noticed that kinetic energy has become time independent at time=20. Kinetic energy becomes constant at $t \geq 20$ (total kinetic energy =1484.113) ie. Solution reaches steady state condition. Fig. 8(b) shows the kinetic energy at steady state. Authors feel that the kinetic energy measure can also be a criterion for checking the convergence. The primary vortex center is acting like in viscid core. Minimum stream function value at primary vortex center is presented in Table II. It is noticed that when *Re* is increased the stream- function value is decreased upto *Re* = 400. Further it is increased. Similar oscillations can be found from Ghia et al. [4]. Primary vortex center moves in the x direction when *Re* is increased and stable at location x = 0.69 for $Re \geq 400$. The primary vortex center location is not varied for $Re \geq 600$. Table III shows the minimum stream function value at the secondary vortex center near the left wall. It is noticed that the values are continuously increased for higher *Re*. The secondary vortex center near right wall is shown in Table IV. The streamfunction values are increased when *Re* is increased. Its vortex center location is oscillating around x = 0.7 in x direction. Tertiary vortex is forming at *Re* = 1300. Its location and minimum streamfunction value are shown in Table V- Table VI.

Effect of *Re* on streamline contour is presented in Fig. 9. At *Re*=1 (Fig. 9(a)) the convection equals the diffusion of the flow. Three vortexes are shown in Figure. Primary vortex whose center locates close to x = 0.5. The secondary vortex forms lower part of the L-shape. Another small secondary vortex forms near left corner of the step. When *Re* increases this small vortex size is increased and its center moves towards the top of the wall (9(b)-9(f)). It is noticed that when *Re* is increased the primary vortex center moves towards right side wall and further it moves and locates near to the intersection of CL1 and CL2 (Fig. 9(f)). It is noticed that at *Re* = 1300 tertiary vortex is forming near the lower part of the domain. The streamtrace is presented for different Reynolds number from Figure 10(a) - Figure 10(d) to show the direction of vortices. It is observed that the primary vortex is rotating in the clockwise direction whereas the secondary vortices are rotating in the counter clockwise direction. u velocity variation for different *Re* is shown in Figure 11(a)-11(d). It is noticed that when *Re* is increased the positive value of u is increased. The u velocity contour in the secondary vortex is increased for higher *Re* values.

The effect of *Re* in minimum streamfunction value at primary vortex is shown in Figure 12. It is noticed that the ψ_{min} value is increased in non-linear manner. A kink is noticed at *Re* = 300.

Walls are the sources of vorticity. Along moving wall $v = 0$ vorticity is due to $-\frac{\partial u}{\partial y}$. The skin friction coe±cient can be related with this velocity gradient $(C_f Re/2 = \frac{\partial u}{\partial y})$. The parameter *CfRe* along *x* direction is shown in Figure 13. The *CfRe* value is increasing along the moving plate upto $x = 0.5$ and further it is decreased. When *Re* is increased the *CfRe* value is increased. It is noticed that the variation of this value for higher *Re*, is significant near the upstream of the moving plate. In the downstream it becomes independent of Reynolds number. This is attributed by the deep cavity at this length.

5. CONCLUSIONS

Two-dimensional incompressible laminar flow in L-shape lid driven cavity is solved for different Reynolds number. The important predictions from the study are as follows. During transient state the primary vortex is forming near the top wall and moves in the plate direction and further it moves in the downstream direction. When *Re* is increased the primary vortex center moves and locates towards the intersection of CL1 and CL2. At $Re \geq 600$ primary vortex center becomes independent of Reynolds number. The counter rotating vortexes are forming at extreme left of the wall and bottom of the split. When Reynolds number is increased the resultant velocity vector strongerμ in the primary vortex region. Moving wall vorticity is significant near the upstream of the moving wall. The skin friction coefficient is sensitive upto $x = 0.5$ and further less significant in the downstream.

Table I Grid independence study: *Re* =400

Grid points	φ_{min} at Primary vortex
41X41	-0.0846
61X61	-0.0849
81X81	-0.0853
101X101	-0.0855
121X121	--0.0855

Table II Minimum streamfunction value at Primary vortex centre

Re	*X*	*y*	φ_{min}
1	0.5463	0.8233	-0.0758
100	0.6766	0.8091	-0.0808
200	0.77053	0.7946	-0.0842
300	0.7053	0.7649	-0.0853
400	0.6908	0.7649	-0.0855
500	0.6908	0.7649	-0.0855
600	0.6908	0.7900	-0.0854
700	0.6908	0.7900	-0.0852
800	0.6908	0.7500	-0.0851
900	0.6908	0.7500	-0.0850
1000	0.6908	0.7500	-0.0848
133	0.6908	0.7500	-0.0845

Table III Minimum streamfunction value at secondary vortex near left wall

Re	X	y	φ_{min}
1	0.0200	0.5200	2E-006
100	0.0276	0.5255	3E-006
200	0.0579	0.5388	2.4E-005
300	0.1482	0.6003	0.00039
400	0.1767	0.6363	0.0014
500	0.1767	0.6766	0.0026
600	0.1909	0.6908	0.0036
700	0.1909	0.7200	0.0045
800	0.1909	0.7350	0.0052
900	0.1909	0.7350	0.0058
1000	0.1779	0.7499	0.0063
1300	0.1767	0.7649	0.0076

Table IV Minimum streamfunction value at secondary vortex near right wall

Re	X	y	φ_{min}
1	0.7606	0.2207	0.0004
100	0.7670	0.7699	0.0002
200	0.7712	0.2205	0.0008
300	0.7649	0.2651	0.0019
400	0.7499	0.2799	0.0030
500	0.7350	0.2947	0.0039
600	0.7201	0.2947	0.0046
700	0.7053	0.2947	0.0052
800	0.7053	0.3092	0.0057
900	0.6908	0.3092	0.0061
1000	0.6908	0.3092	0.0064
1300	0.6765	0.3092	0.0072

Table V Minimum streamfunction value at tertiary vortex near left wall

Re	X	y	φ_{min}
1300	0.0149	0.5173	-9.094E-007

Table VI Minimum streamfunction value at tertiary vortex near right wall

Re	X	y	φ_{min}
1300	0.5170	0.0189	-8.165E-007

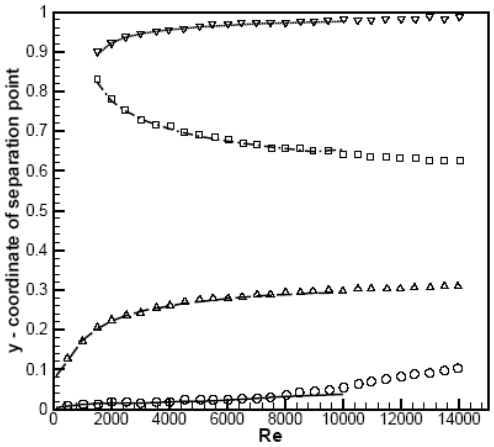

Figure 2 Lid driven flow problem [4]. Left wall sepration points. Open symbols [15] and line patterns-present results.

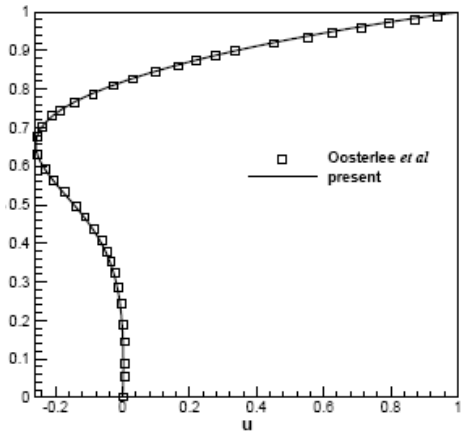

(a) *u* Velocity (CL1), *Re*=100

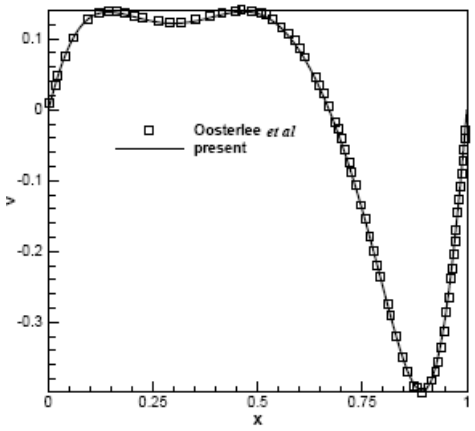

(b) *u* Velocity (CL2), *Re*=100

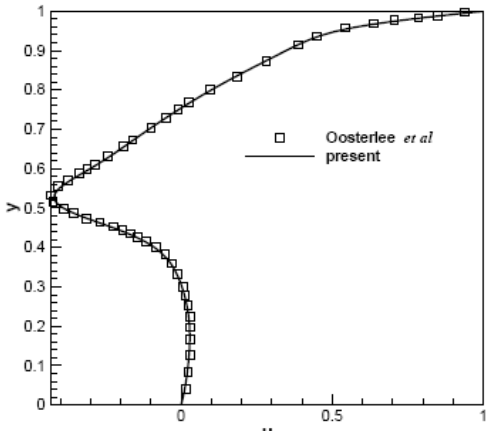

(c) *u* Velocity (CL2), *Re*=1000

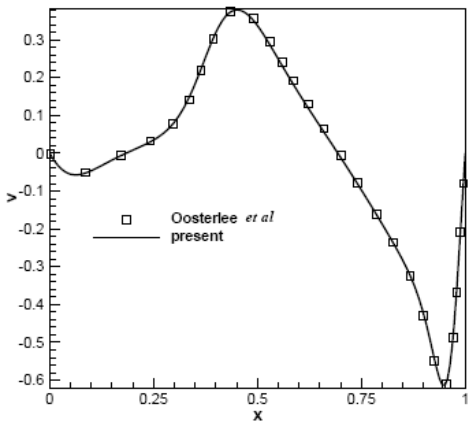

(d) *u* Velocity (CL2), *Re*=1000

Figure 3 L-shape lid driven cavity flow problem [9]. Velocity profiles along CL1 and CL2

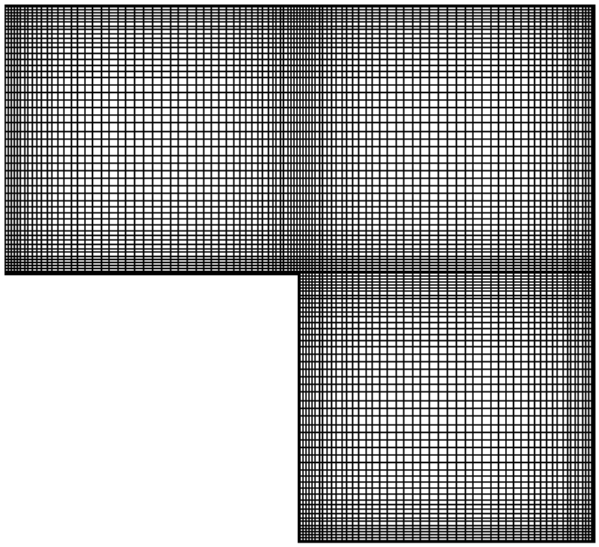

Figure 4 Typical grids used for the computation Δx_{min}=Δy_{min}=0.00501

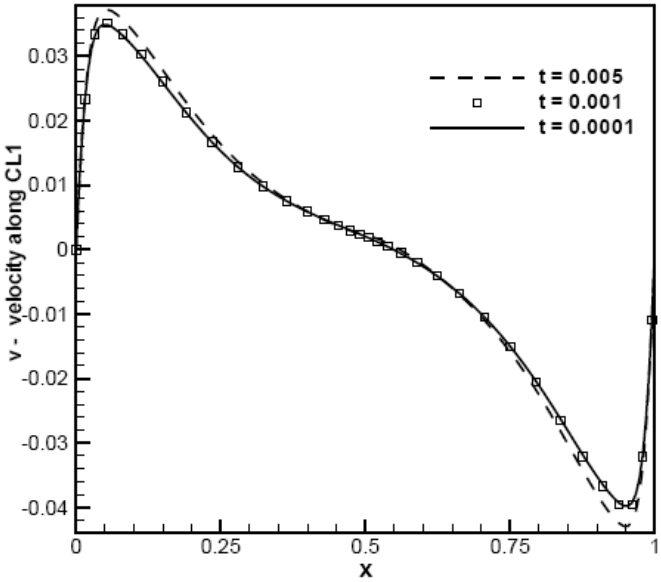

Figure 5 Time independent study u velocity along CL2 *Re*=400, t=0.1

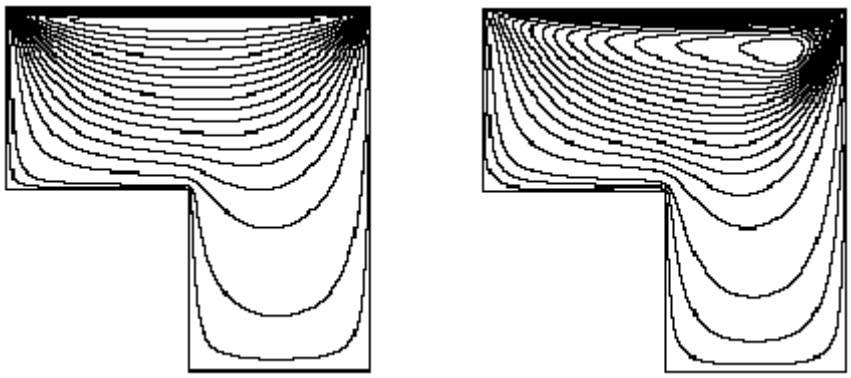

(a) t=0.1 (b) t=1

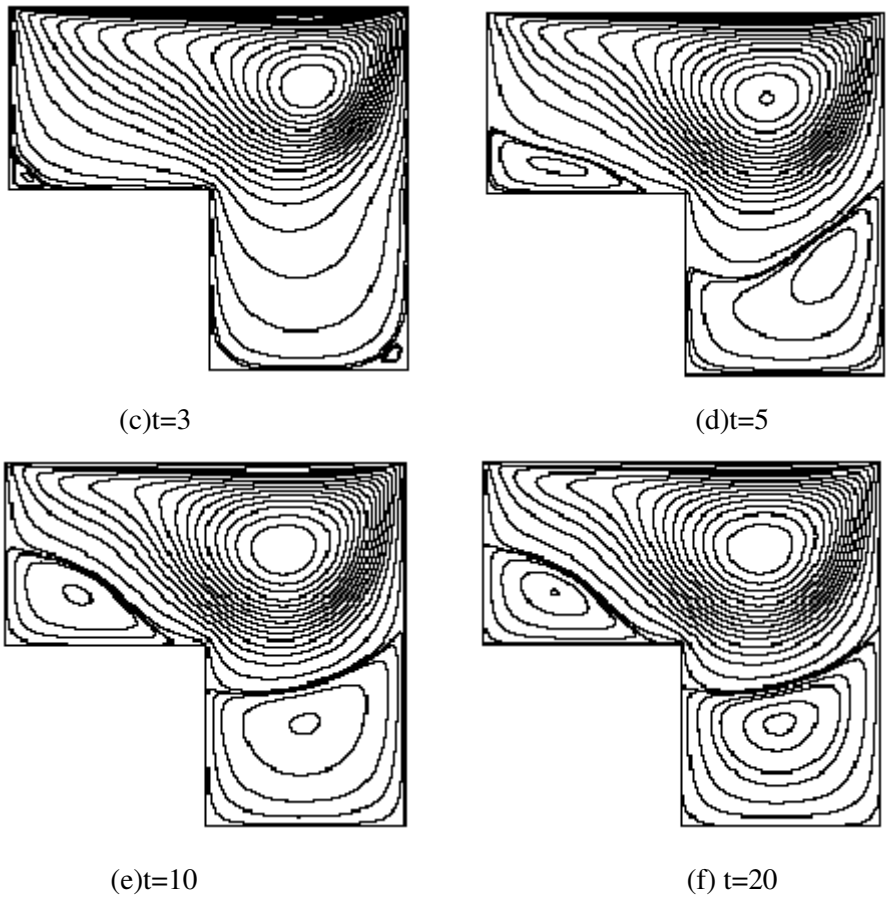

(c)t=3 (d)t=5

(e)t=10 (f) t=20

Figure 6 Transient results streamline contour *Re*=400

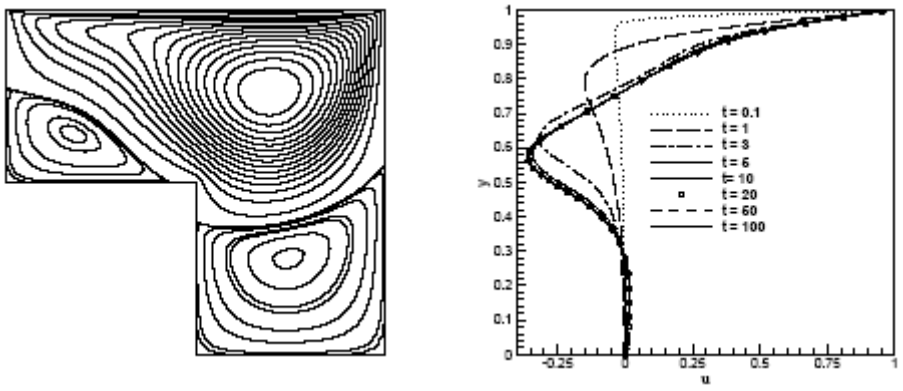

(a)t=100 (b) Transient results u velocity along CL1. *Re*=400

Figure 7 Transient results

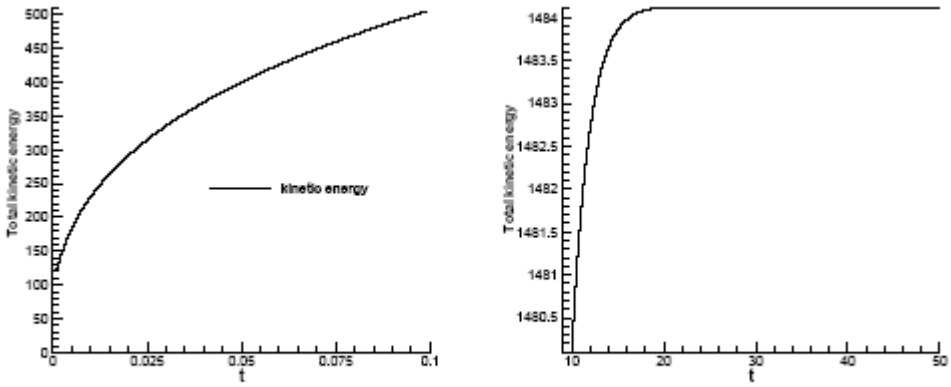

(a) $t \leq 0.1$ (b) $t \geq 10$

Figure 8 Total kinetic energy *Re*=400

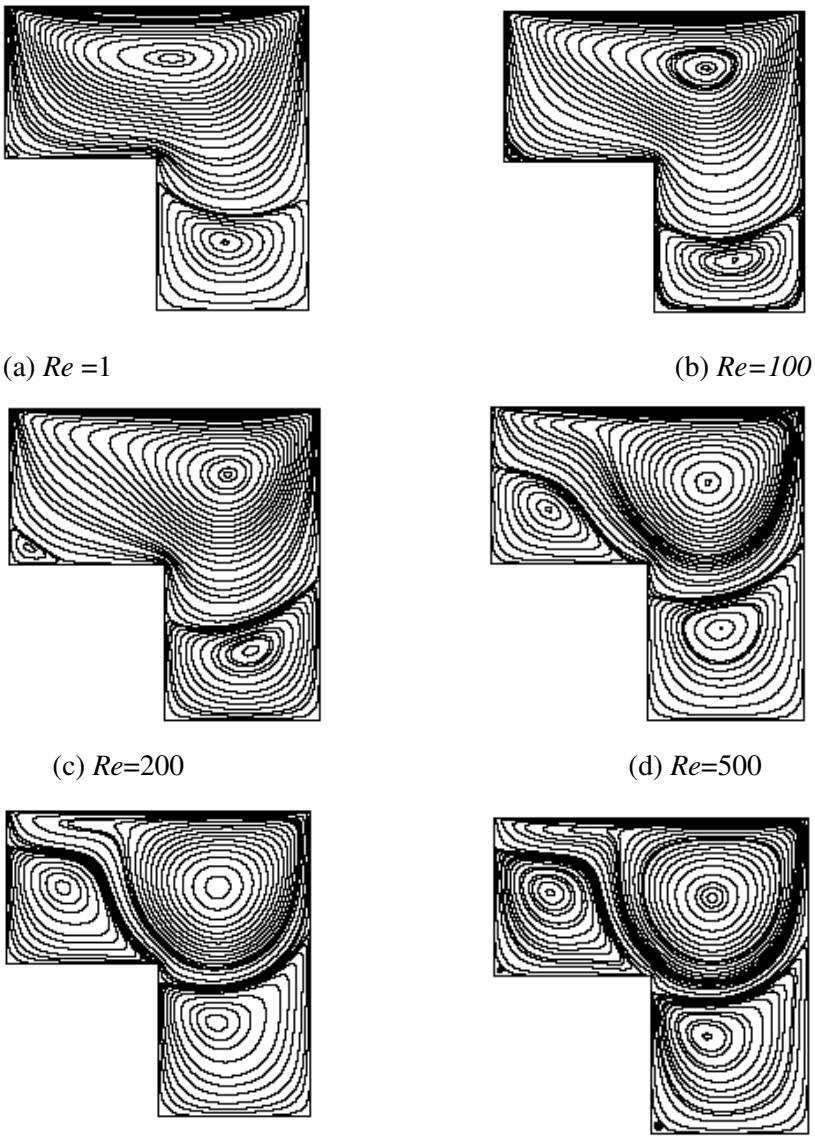

(a) *Re* =1 (b) *Re=100*

(c) *Re*=200 (d) *Re*=500

(e)*Re*=1000 (f)*Re*=1300

Figure 9 streamline contour

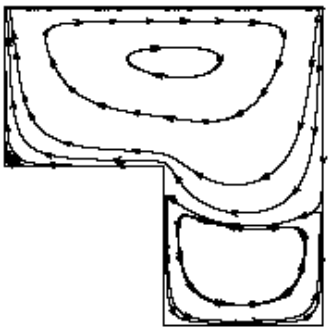

(a)Velocity vector, *Re*=1

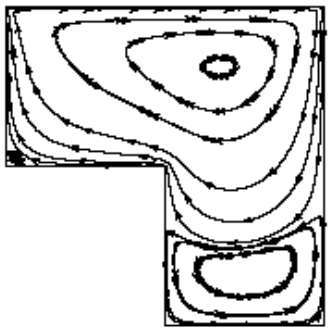

(b) Velocity vector, *Re*=100

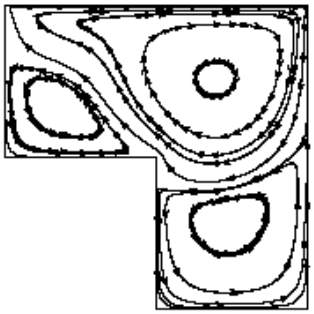

(c)Velocity vector, *Re*=500

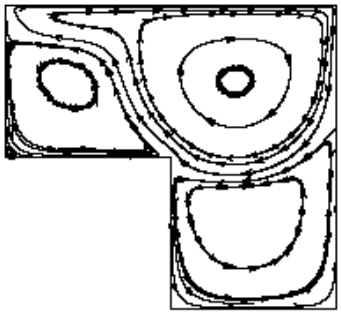

(d) Velocity vector, *Re*=1000

Figure 10 stream trance for different *Re*

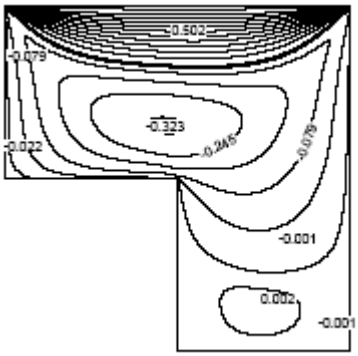

(a) *u* Velocity contour, *Re*=1

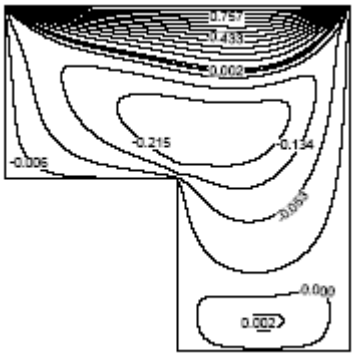

(b) *u* Velocity contour, *Re*=100

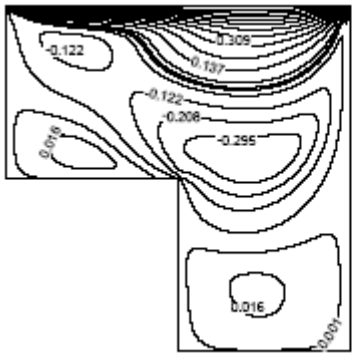

(c) *u* Velocity contour, *Re*=500

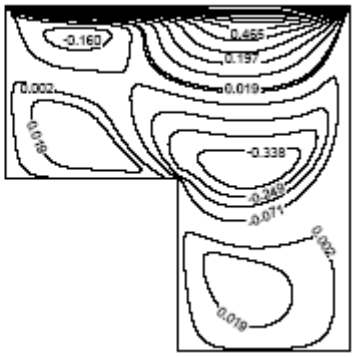

(d) *u* Velocity contour, *Re*=1000

Figure 11 velocity contour

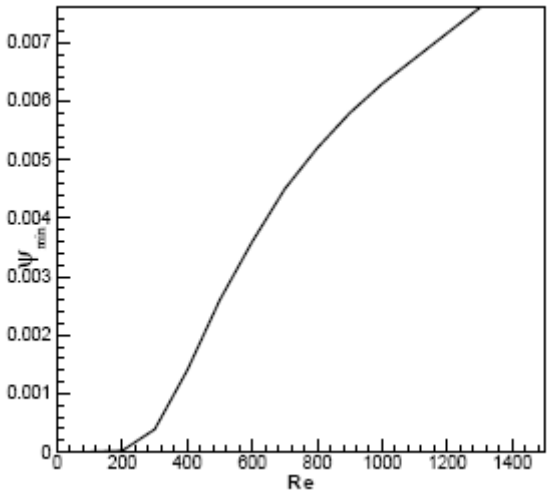

Figure 12 Variation of minimum streamfunction value for different Reynolds number

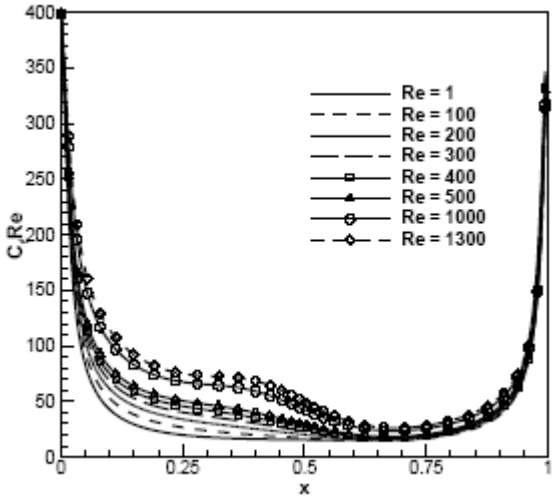

Figure 13 Skin friction coefficient for different *Re*

REFERENCES

[1] Shohel Mahmud. Free convection inside an l-shaped enclosure. *Int. Communication in Heat Mass Transfer*, 29.1005-1013, 2002.

[2] O.R. Burggraf. Analytical and numerical studies of the structure of steady separated flows. *Journal of Fluid Mechanics*, 24.113-151., 1966.

[3] M. Nallasamy and K.K. Prasad. On cavity flow at high Reynolds numbers. *Journal of Fluid Mechanics*, 79(2).391-414, 1977.

[4] U. Ghia, K.N. Ghia, and C.T. Shin. High Re solutions for incompressible flow using the Navier-Stokes equations and multigrid method. *Journal of Computational Physics*, 48.387-411, 1982.

[5] A.B. Cortes and J.D. Miller. Numerical experiments with the lid driven cavity flow problem. *Computers and Fluids*, 23.1005-1027, 1994.

[6] S-J Liao and J-M Zhu. A short note on high-order streamfunction-vorticity formulations of 2d steady state Navier-Stokes equations. 95.228-245, 1991.

[7] H. F. Oztop and I. Dagtekin. Mixed convection in two-sided lid-driven differentially heated square cavity. *International Journal of Heat and Mass Transfer*, 47.1761-1769, 2004.

[8] B. Podvin, Y. Fraigneau, F. Lusseyran, and P. Gougat. A reconstruction method for the flow past an open cavity. *ASME Transactions Journal of Fluids Engineering*, 128.531-540, 2006.

[9] C.W. Oosterlee, P. Wesseling, A. Segal, and E. Brakkee. Benchmark solutions for the in-compressible navies-stokes equations in general co-ordinates on staggered grids. *International Journal for Numerical Methods in Fluids*, 17.301-321, 1993.

[10] S. Kulsri, M. Jaroensutasinee, and K. Jaroensutasinee. Simulation of lid cavity flow in rectan-gular, half-circular and beer bucket shapes using quasi-molecular modeling. *World Academyof Science, Engineering and Technology*, 33, 2007.

[11] P.J. Roache. Fundamentals of Computational Fluid Dynamics, chapter-3. Hermosa, USA, 1998.

[12] P.R. Kanna and M.K. Das. Numerical simulation of two-dimensional laminar incompressible offset jet flows. *International Journal for Numerical Methods in Fluids*, 49.439-464, 2005.

[13] R.A. Kuyper, Th.H. Van Der Meer, C.J. Hoogendoorn, and R.A.W.M. Henkes. Numerical study of laminar and turbulent natural convection in an inclined square cavity. *International Journal of Heat and Mass Transfer*, 36(11).2899-2911, 1993.

[14] G. Comini, M. Manzan, and C. Nonino. Finite element solution of the streamfunction-voriticity equations for incompressible two-dimensional flows. *International Journal for Nu-merical Methods in Fluids*, 19.513-525, 1994.

[15] E. Barragy and G.F. Carey. Stream function-vorticity driven cavity solution using *p fi*nite elements. *Computers and Fluids*, 26(5).453-468, 1997.

[16] P.R. Kanna and M.K. Das. Numerical simulation of two-dimensional laminar incompressible wall jet under backward-facing step flows. *ASME Transactions Journal of Fluids Engineering*, 128.1023-1035, 2006.

[17] O. Goyon. High-reynolds number solutions of Navier-Stokes equations using incremental un-knowns. *Computer Methods in Applied Mechanics and Engineering*, 130.319-335, 1996.